SIS Monitoring for ARAIM in the Absence of Precise Clock Estimates

Kazuma Gunning, Todd Walter, David Powell – *Stanford University*

ABSTRACT

This paper describes methods for constellation monitoring in the absence of external precise clock estimates. Careful characterization of constellation performance is necessary for the use of Advanced RAIM (ARAIM). In particular, the narrow (P_{sat}) and wide (P_{const}) fault rates must be determined. However, typical constellation monitoring approaches rely on the comparison between the broadcast ephemeris and precise estimates of the satellite orbit and clock, and these may not always be available. Furthermore, they may only monitor reference signals that will not actually be operationally used. This paper describes a method to independently estimate satellite clock and differential code biases in order to evaluate the ranging performance of GPS and GLONASS for ARAIM. Daily variations in the L1 C/A-L5Q clock and differential code bias are examined and quantified. Finally, GLONASS faults are closely examined using the clock estimation techniques.

INTRODUCTION

The use of a GNSS in Advanced RAIM requires the careful, long-term characterization of its signal-in-space (SIS) performance. Traditional methods do this characterization through the comparison of the broadcast navigation message to precise estimates of the satellite orbit and clock, which are generated by the International GNSS Service (IGS) or National Geospatial-Intelligence Agency (NGA). The results of this approach can be seen in Figure 1, which shows the performance history of GPS from 2008-2018, including the five observed fault events.
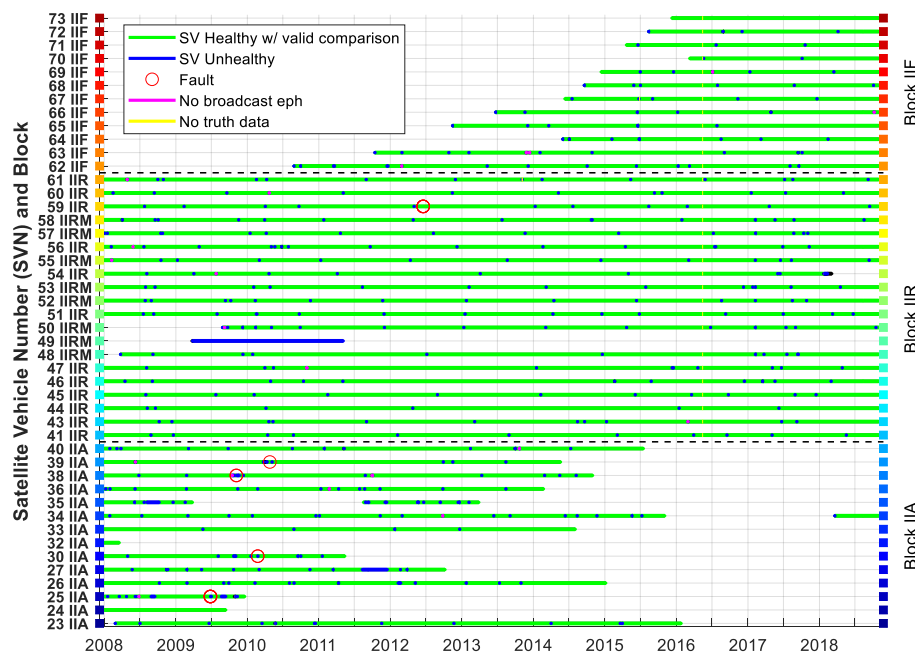

Figure 1: GPS Constellation Performance Overview comparing broadcast navigation message to NGA precise orbit and clock: 2008-2018

However, when these precise estimates are unavailable, these methods fail. If a satellite is observed to be broadcasting a ranging signal with a valid navigation message, it is important that its performance is assessed

during that period, regardless of the availability of external precise products. This paper provides methods for fault detection and nominal performance characterization in the absence of external precise clock estimates.

The overall goal of such a constellation monitoring system is the long-term characterization of constellation performance.   In particular, ARAIM Integrity Support Message (ISM) parameters such as P_{sat} (probability of satellite fault), P_{const} (probability of constellation fault), and bounding User Range Accuracy (URA) sigmas are of interest. Previous papers [1] have described methods of estimating these parameters over long periods and rely heavily on the availability of IGS precise products. However, it has been shown that such precise products are not always available, even during periods where faults have been observed [2] [3]. The goal of IGS analysis centers is accuracy, not necessarily 100% availability, so when anomalous behavior by the satellite is detected, an estimate may not be output. While nominal statistics may not be affected by occasional outages in the precise clock and orbit data, more sensitive parameters such as P_{sat} and P_{const} can be significantly impacted by missing periods of precise data. In addition to data that is missing at times, some products, such as differential code biases (DCB), are only updated at most on a daily basis by the IGS analysis centers [4]. DCB's, or the corresponding GPS term, the inter-signal corrections (ISC), are required for an ARAIM dual frequency solution. Because of this, the careful characterization of these DCB's is important. This paper serves to provide methods to increase the availability of constellation monitoring such that the performance of a satellite can be assessed whenever it is observed to be broadcasting a ranging signal.

The approach described in this paper is to estimate the GNSS clock biases for a dual frequency reference signal as well as estimate DCB's for additional dual frequency signal pairs of interest. When evaluating constellation performance for ARAIM, the L1 C/A – L5 combination is what we focus on. The benefits of such a process are multiple. First, this allows for the analysis to be decoupled from the IGS clock estimates, which may not be 100% available when anomalous behavior is present. Even when IGS estimates are available, this allows for validation of those values. This also allows for analysis that is at a higher rate than is currently available from the IGS analysis centers. For example, GLONASS clock bias estimates are not available at rates higher than 30 seconds. Finally, and perhaps most importantly, the signals combinations of interest can be monitored long term, whereas they have not been properly examined thus far. While GPS DCB's are generally stable, they have been observed to have changed rapidly when flex power is used [5]. With current IGS DCB products, the immediate impacts on ranging accuracy cannot be assessed.

The clock and DCB estimation process is driven by a ground network of multi-constellation, multi-frequency receivers that are members of the IGS Multi-GNSS Experiment (MGEX) [6] network. Given known positions of the receivers and satellites as well as careful modeling of the range measurements, estimates of the receiver clock biases, satellite clock biases, tropospheric states, carrier phase ambiguities, and DCB's are produced. The general estimation strategy relies on a low rate batch least squares over long periods and then handing over results from that first estimate to a single epoch estimate of the various clock biases and DCB's.

CLOCK BIAS AND DCB ESTIMATION

This section describes the general approach to and results from the Stanford University (SU) clock bias and DCB estimation process.

Ground receiver selection

The ground receivers used in the clock and DCB estimation process are selected from the full set of over 200 IGS MGEX receivers. Using the full set of receivers would require more processing power than desired and provide only marginally improved estimation performance over using a subset. In addition, not all receivers even track the signals of interest, making them useless for our purposes.   Because of this, we implemented a

very simple receiver selection algorithm that allows the clock estimation system to be automated and efficient even as the available receivers changes over time.
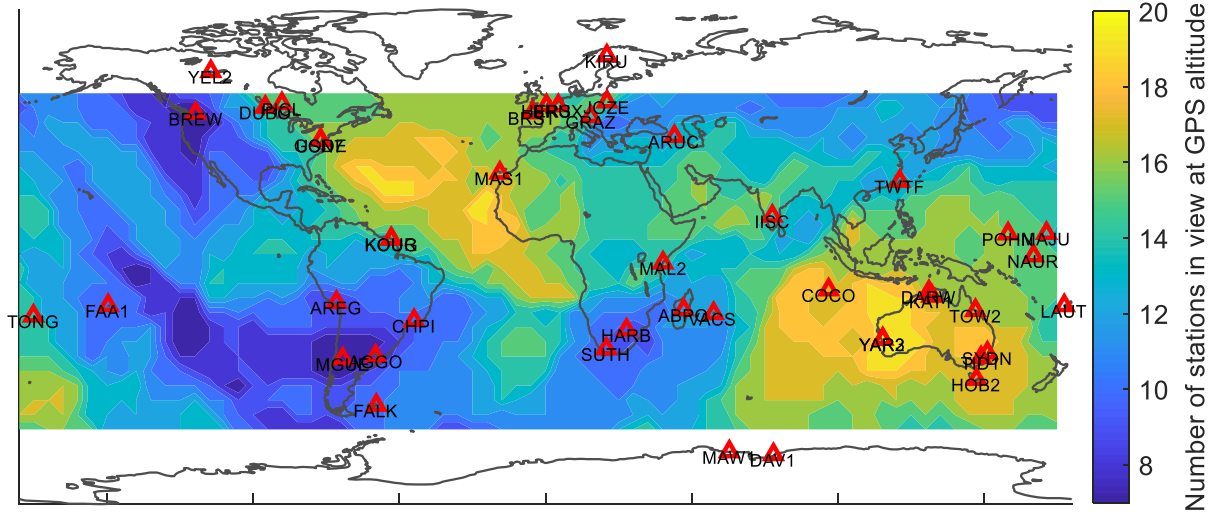

Figure 2: Number of ground receivers in view at GPS altitude

The algorithm is a very simple greedy algorithm that first creates a globally distributed grid of "users" at the orbital altitude of the constellation of interest. These users only span from the negative to the positive latitude corresponding to the inclination of the orbits of the constellation of interest. For example, the inclination of the GPS orbits is 55°, so the user grid excludes any users above or below 60° latitudes, where 60° is chosen to have some margin. Ultimately, the station selection is not incredibly sensitive to the amount of margin chosen. From here, given our empty station list, the number of users in view from each station is counted, and the station with the most users in view is added to the station list. The number of stations in view from each user is updated with our new station list. The process is repeated, where the additional visibility from each user is computed, except that users with fewer stations in view are weighted more heavily when choosing the new station. This continues until the minimum number of stations in view is reached. In Figure 2, the minimum number of stations in view for any user location on orbit is seven, ensuring significant redundancy in the clock and DCB estimates.

Measurement modeling

Dual frequency code and carrier phase measurements are the primary inputs to the estimator. How exactly the measurements are modeled, i.e. what delays are computed deterministically using models and what are estimated, is very important. The basic pseudorange and carrier phase measurement models are as follows:

Dual frequency carrier phase:
$$\Phi_{if}^{(i)} = \left\| x_s^{(i)} - x_{rx} \right\| + c \left(\hat{b}_{rx,c} - \hat{b}_s^{(i)} \right) + m^{(i)} \widehat{\Delta T}^{(i)} + \widehat{DCB}_s^{(i,k)} + \widehat{DCB}_{rx}^{(k)} - \hat{A}^{(i,k)} + \mathrm{R_m} + \epsilon$$
(1)

Dual frequency code phase:
$$\rho_{if}^{(i)} = \left\| x_s^{(i)} - x_{rx} \right\| + c \left(\hat{b}_{rx,c} - \hat{b}_s^{(i)} \right) + m^{(i)} \widehat{\Delta T}^{(i)} + \widehat{DCB}_s^{(i,k)} + \widehat{DCB}_{rx}^{(k)} + \mathrm{R_m} + \epsilon$$
(2)

Where

$x_s^{(i)}$- satellite position provided by external precise orbit product

$\hat{x}_{rx}$- known receiver position from IGS daily solution

$\hat{b}_{rx,c}$- estimated receiver clock bias

$\hat{b}_s^{(i)}$- estimated satellite clock bias

$m^{(i)}$- tropospheric mapping function

$\widehat{\Delta T}^{(i)}$- estimated delta tropospheric delay

$\hat{A}^{(i,k)}$- estimated float carrier phase ambiguity

$\widehat{DCB}_s^{(i,k)}$- estimated satellite differential code bias per signal (one per SV and non-reference signal)

$\widehat{DCB}_{rx}^{(k)}$- estimated receiver differential code bias per signal (shared across SVs)

R_m- Other modeled effects. This includes relativistic effects, solid earth tide modeling, satellite antenna phase center offset and variation, ocean loading, modeled tropospheric delay, and carrier phase windup. These are strictly deterministic and not estimated.

ϵ - other unaccounted for errors- this should be zero mean and Gaussian, essentially reflecting measurement noise.

The estimated states include the receiver clock biases, satellite clock biases, tropospheric delay delta, differential code biases for each satellite and signal, differential code biases for each receiver and signal, and carrier phase ambiguities for each carrier phase measurement. There only a few differences between this measurement modeling and that of traditional Precise Point Positioning (PPP). Namely, that receiver position is not estimated, and that satellite clock biases and DCBs are. For a single receiver, these states would of course be unobservable, but with a network of receivers, they can be happily estimated.

Evaluating L1 C/A-L5Q Ranging

Satellite hardware causes varying delays for each signal being broadcast. These delays are typically called the differential code bias; the GPS interface specifications call the terms that describe the delays inter-signal corrections (ISC). One of the goals of this paper is to evaluate the impact on ranging of these delays on the ARAIM user. The ranging impact is explored in two ways. The first method is to estimate a new clock state using the L1 C/A-L5Q dual frequency code and carrier measurements. This allows for a very similar analysis to what has been done previously, where instead of using IGS precise clock, which use the L1P-L2P dual frequency combination, the SU estimates can be used. In the analysis in this paper, the difference between the clock bias estimated using L1 C/A and L5Q and the clock bias estimated using L1P-L2P will be primarily examined and compared to broadcast parameters.

However, the ARAIM navigation solution uses carrier-smoothed code, so it is very important to examine the ranging impact of using pseudoranges directly. To do this, differential code biases are estimated for the L1 C/A-L5Q combination. Because they are pseudorange-based and thus very noisy, the estimates are averaged over some time span. In this paper, we use a daily 24-hour interval for validation and finally use a 15-minute interval estimate.

The broadcast timing offset to use the L1 C/A – L5 Q combination is found from the following, per IS-GPS-705D [10]:

$$PR = \frac{\left(PR_{L5Q5}-\gamma_{15}PR_{L1C/A}\right)+ c\left(ISC_{L5Q5}-\gamma_{15}ISC_{L1C/A}\right)}{1-\gamma_{15}} - cT_{GD} \tag{3}$$

The combination of corrections that is compared to the SU estimated DCBs is then:

$$DCB_{L1C/A-L5Q5} = \frac{c\left(ISC_{L5Q5}-\gamma_{15}ISC_{L1C/A}\right)}{1-\gamma_{15}} - cT_{GD} \tag{4}$$

When using any signal combination that is not L1P-L2P, some combination of ISCs must be used. In this paper, we compare the measured ranging difference for the L1 C/A-L5Q combination to the broadcast terms that are meant to capture this offset. Ultimately, it is the left hand side term in equation 4 that is compared to the clock bias difference or the differential code bias. Figure 3 summarizes all of this. The smooth black line at the bottom is the carrier phase-estimated primary clock estimate for the L1P-L2P combination. The red line is a new clock estimated for the L1 C/A –L5Q combination, also estimated using code and carrier. The noisy grey line is the differential code bias. We compare the difference between the red line (clock) or the grey line (DCB) and the black line to the broadcast DCB.
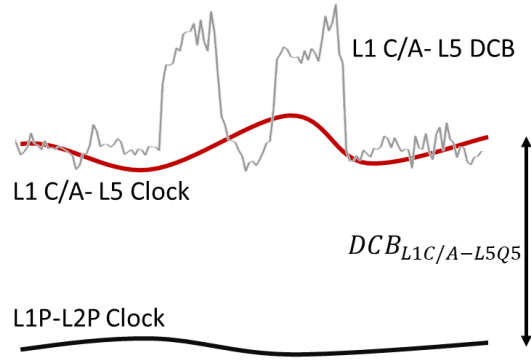

Figure 3: Clock differences and differential code biases

The broadcast DCB terms have been provided by IGS MGEX logs of the CNAV messages. Figure 4 shows the DCB terms throughout 2018 for each of the block IIF satellites, which are the only satellites broadcasting on L5. The DCB's are largely stationary through the year.
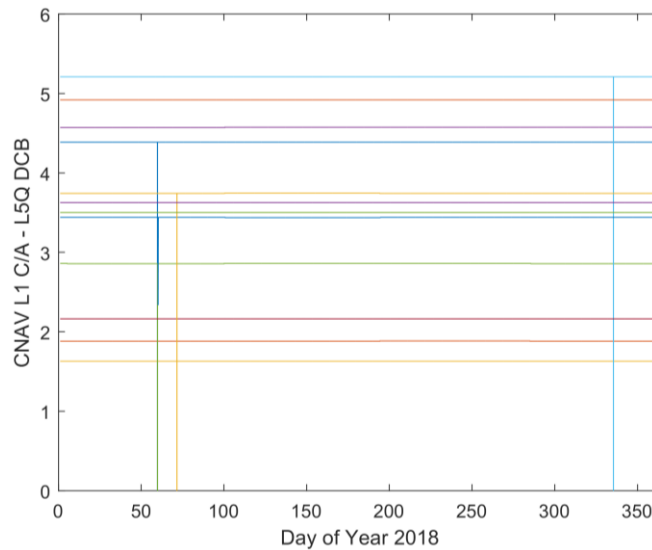

Figure 4: GPS CNAV Values of L1 C/A- L5Q Dual Frequency DCB

Estimation structure

The estimation approach is to use a low rate batch weighted least squares to estimate carrier phase ambiguities and tropospheric delays across the network of ground station network, then to freeze those estimates and at each epoch, make the final estimates of the various clock and code biases.

The initialization process first requires producing satellite positions for all satellites and times in order to mask measurements from low-elevation satellites. The position of the sun is also precomputed for all times; this is used in the satellite attitude computation for the antenna phase center offset. Antenna phase centers are provided by the IGS [7], and nominal attitude models are used [8]. The effect of these nominal models on the estimation performance when the satellites are in eclipse conditions will need to be investigated in the future. Next, the carrier phase measurements are processed. Cycle slips are detected using a simple test on the change in the geometry-free combination of the two carrier phase measurements that make up the dual frequency observations. Carrier phases are collected into continuous arcs, and only arcs of length exceeding a minimum threshold are kept, and the other measurements are discarded. All of the code phase measurements are kept.

A single batch least squares estimate of all of the desired parameters over all times is not feasible from a memory standpoint, so the estimation is broken into three parts. The first two parts, the "slow" estimator, does estimate all of the desired parameters but only at a low rate, i.e. 5 or 15 minutes between epochs. The first part, the state initialization, does an extremely rough (~200 m accuracy) estimate of the station and satellite clock states using only pseudoranges and no range error modeling. This is done simply to reduce the number of iterations of the precise slow estimator. The states in the precise slow estimator are as follows:

> *Receiver clock bias*: one per station and epoch
> *Satellite clock bias*: one per satellite and signal pair and epoch
> *Tropospheric delay*: one per station and slowly changing over time
> *Satellite differential code bias*: one per SV, epoch, and non-reference dual-freq. signal combination
> *Receiver differential code bias*: one per station and non-reference dual-freq. signal combination- this
>   is constant over time.

The reference dual-frequency signal pair used for GPS is the L1 P-L2 P semi-codeless combination, as is used by both the IGS and the GPS broadcast navigation messages. As such, this combination does not require a satellite differential code bias.

The estimator loops through each station and epoch in order to build the sensitivity matrix for the iterative weighted least squares process. The weights are simply a standard σ values for code and carrier phase scaled for the elevation angle. This scaling helps to capture the error due to multipath as well as, more importantly for the carrier phase measurements, the error in the precise orbit estimates, which are projected more heavily onto the line of sight of the measurement at low elevation angles. This estimator does not start with any prior estimates of the receiver or satellite clock biases, which leads to generally needing at least two iterations of the least squares process to converge.

Once the slow estimation is complete, the high rate estimation can occur with the now-frozen carrier phase ambiguities and tropospheric delays. This approach is favorable when compared to doing one enormous iterative least squares because the size of the matrices involved when estimating separately for each epoch do not change, whereas the size of the matrices involved in a batch estimate increase exponentially. This means that high rates become infeasible for the single batch estimates. For the high rate estimation, a very similar approach is taken to that of the low rate, except that interpolated estimates of the clock biases from the slow estimate are used to seed the process.
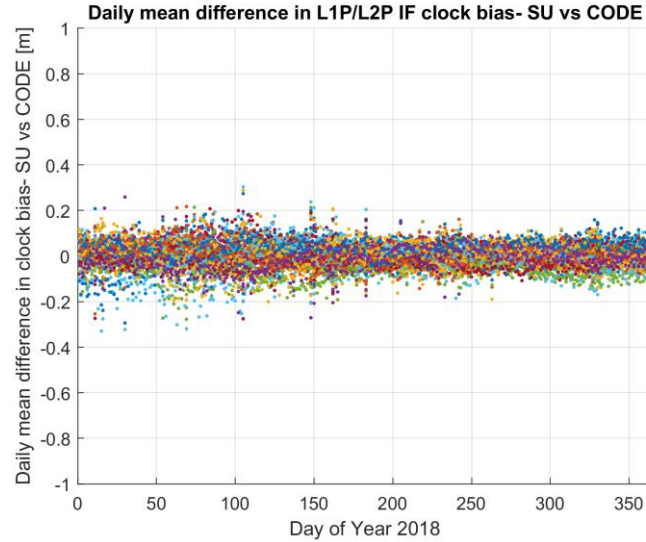
L1P-L2P Clock Estimation Results

Figure 5: Comparison of SU GPS vs IGS CODE clock bias estimation for 2018

The first set of results is a comparison of the clock output by the SU estimator to that of an IGS analysis center, the Center for Orbit Determination European (CODE). The CODE product is output at 5 second intervals and is centimeter-level accurate. As with all IGS GPS clock products, the reference observables are the L1P and L2P code and carrier, so we compare the CODE clock to our L1P-L2P clock estimate. Figure 5 shows this comparison, where the clock estimate for each satellite is compared to that produce by CODE, and a mean for each day of 2018 is produced for each satellite. Each of the colored dots in Figure 5 is a separate satellite and day of 2018. The RMS of the error across all satellites and days is 7 cm, and the daily mean difference never exceeds 35 centimeters over the year. This result is meant simply to be validation of the estimation techniques and data handling so that further results can be trusted.
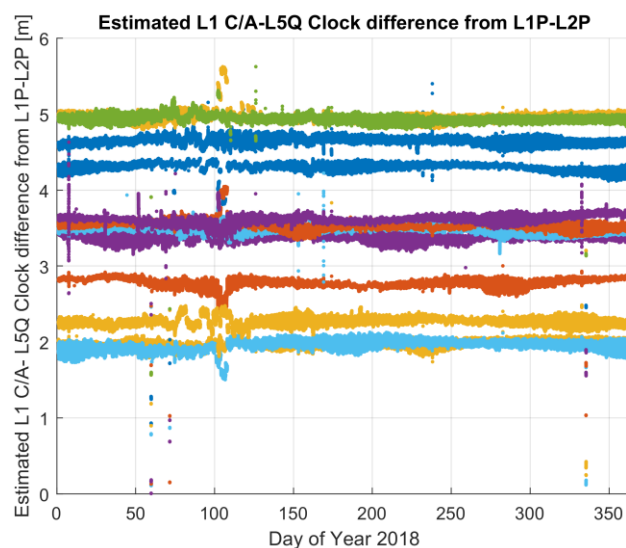
L1 C/A- L5Q Clock Estimation Results

Figure 6: SU Estimated L1 C/A - L5Q Difference from L1P-L2P

This section examines clock bias difference between the L1P-L2P dual frequency combination and the L1 C/A-L5Q dual frequency combination. Figure 6 shows just the difference in clock bias between the two dual frequency pairs as produced by the SU estimator. Each GPS Block IIF satellite is shown as a different set of colored dots. As expected the clock differences are largely static through the year, but there is a noticeable "swelling" of the clock differences that changes throughout the year that is more prominent on some satellites than others. The values shown in this figure are what will be compared to estimates of the same values produced by the German Aerospace Center (DLR) in Figure 7 as well as broadcast in the GPS CNAV message in Figure 8.
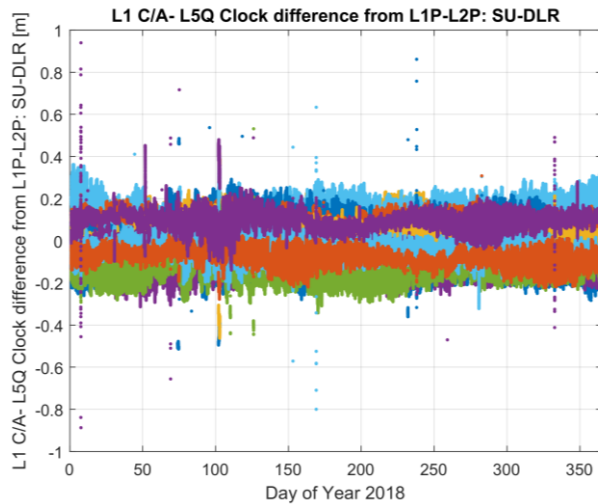
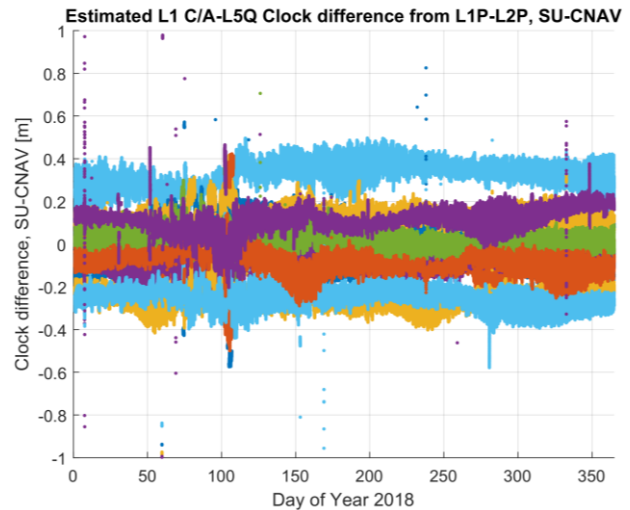*Figure 7: L1 C/A- L5Q Clock Difference from L1P-L2P: SU-DLR*

Figure 8: L1 C/A- L5Q Clock Difference from L1P-L2P: SU-CNAV

Figure 7 shows a comparison between the L1 C/A-L5Q clock offset produced by SU and the offset produced by DLR. The daily DCB estimates produced by DLR were subtracted from the values shown in Figure 6 to, as before, validate the performance of the estimator. The DCB's produced by DLR are for each single frequency signal individually, so they must be combined in the proper manner as in Equation 4. Additionally, they are daily mean values, so the effects of daily variations are still visible. Despite these factors, the SU estimates closely match the DLR estimates, with an RMS difference over the year of only 10 cm. Figure 8 shows a similar comparison that replaces the DLR DCB's with those produced using CNAV message parameters. Overall, the difference remains relatively small, this time showing an RMS difference of 20 cm. However, the mean differences of some of the satellites, in particular SVNs 66 and 67, push up close to 40 centimeters.
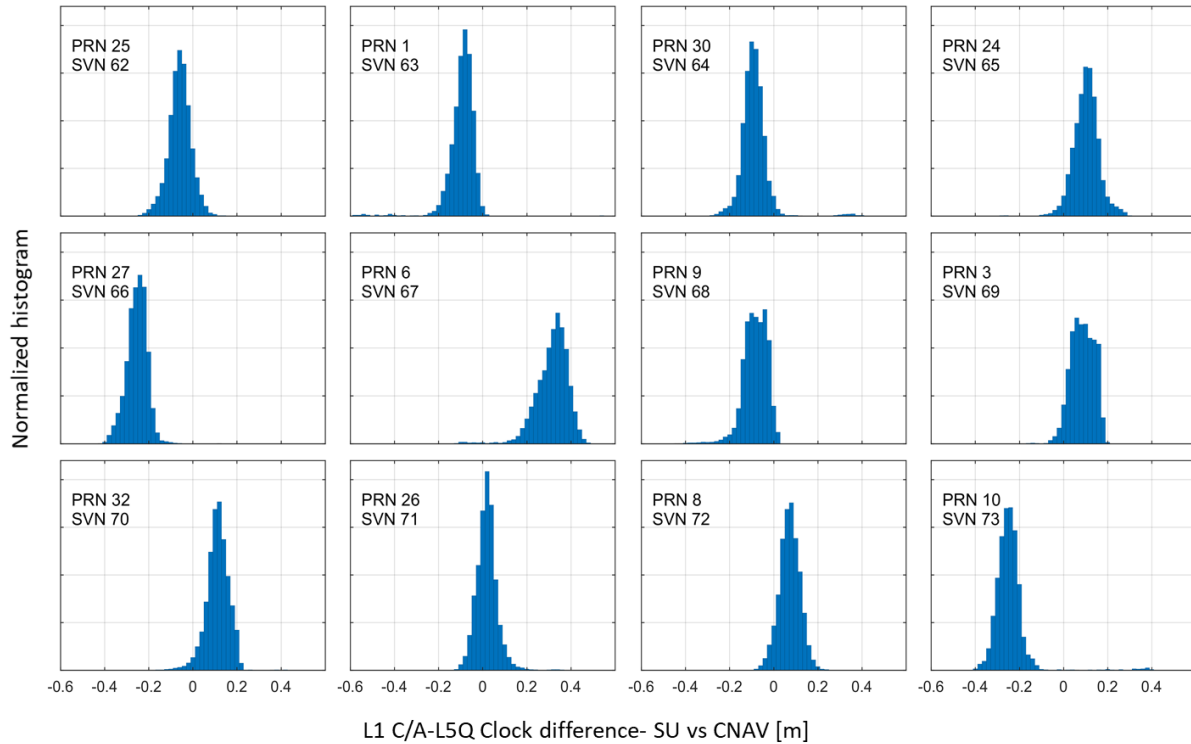
Figure 9: Histogram of L1 C/A- L5Q Clock Difference from L1P-L2P: SU-CNAV

Figure 9 shows the same data as in Figure 8, except this time as a histogram for each satellite individually. The individual distributions are tight, with standard deviations of not more than 10 centimeters for any satellite. The means do approach 40 centimeters in a few cases, as previously mentioned. Ultimately, the effects described in this section are driven by the carrier phase measurements, which are only used for smoothing in ARAIM navigation solutions. Because of this, the impact of the clock difference effects shown here are potentially limited for the ARAIM user.
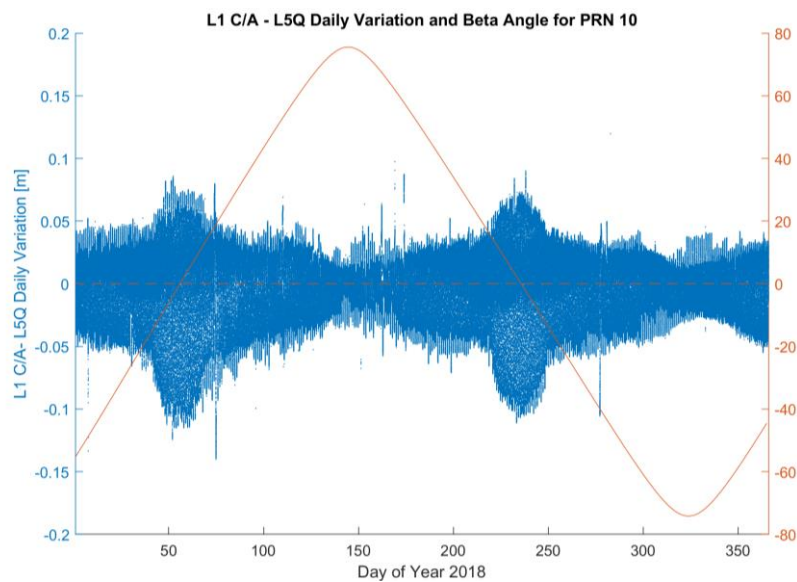

Figure 10: L1 C/A-L5Q Daily Variation and Beta Angle for PRN 10

This section seeks to help explain the daily variations in the clock bias between the L1P-L2P and L1 C/A-L5Q combinations. As they are carrier phase estimates, one might expect that the difference would be extremely stable, but there are noticeable and predictable daily variations. These effects have been observed and described in detail in previous works [13], so this section will be brief. Figure 10 takes the data from Figure 6 for one satellite and for each day removes the mean value. This leaves only the daily variation of the signal, showing very clearly significant changes in the daily variation throughout the year. The red line in Figure 10 is the satellite's β angle, which is the angle between the Sun, the Earth, and the projection of the Sun vector onto the satellite orbital plane. The satellite orients itself so as to maintain a solar panel angle with respect to the sun. At high β angles, very little yaw motion is required to maintain the specified attitude, whereas at low β angles, very rapid noon and midnight turns occur when the satellite passes in front and behind the Earth during the orbit. This yaw motion has been linked to the variations in the clock bias between L5 and other frequencies [13]. Figure 11 illustrates the daily variations at high and low beta angles for PRN 10.
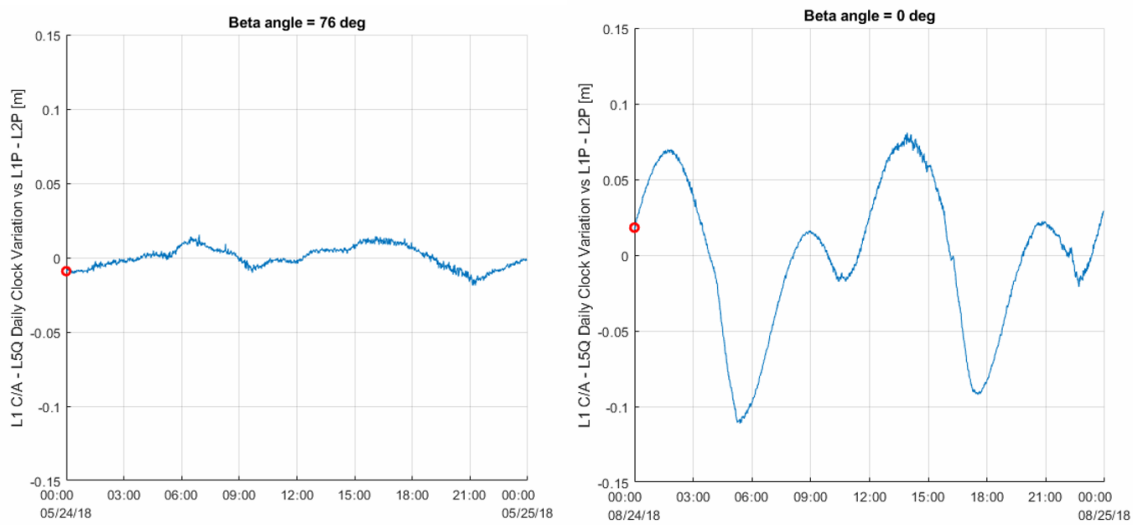

Figure 11: Daily variations in L1 C/A - L5Q vs L1P-L2P clock bias at high and low beta angles

DCB Estimation Results

This section shows results relating to the estimation of the differential code bias between the L1 C/A - L5Q and L1P-L2P dual frequency pairs. The previous section examined the difference in the clock bias between the two signal pairs by using the carrier phase, whereas from now on, the code-only difference will be examined. This is particularly important for ARAIM, as it uses a carrier-smoothed code solution, and the ranging differences are more significant when considering the true differential code bias.
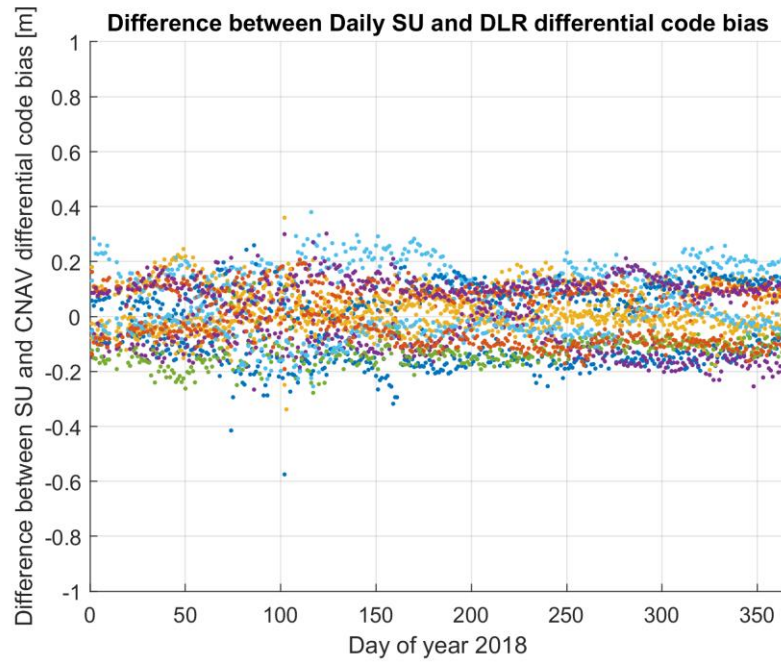
Figure 12: Difference between Daily SU and DLR Differential Code Bias

As before, we seek to validate our results by comparing to known precise estimates of the parameters of interest. In Figure 12, daily estimates of the L1 C/A-L5Q DCB are compared to the daily estimates of the same values produce by DLR. As before, each set of colored dots indicates a different satellite, and there is one dot per day. The SU estimates are, here, produced at 24 hour intervals and are expected to match those produced by DLR. The RMS difference is 11 cm over the one-year time span. Currently, IGS precise estimates of the DCB's are only available at 24 hour intervals at the fastest. However, we, and others [5] have observed changes at higher rates, so we have also produced DCB estimates at 15 minute intervals.

Figure 13 shows a comparison between the high rate SU DCB estimates and the daily DLR DCB estimates. Immediately, it becomes clear that there is significant deviation from the daily average. This deviation is due to more than noise, though the noise on the estimate does increase. The daily deviation is caused largely by the ongoing flex power campaign, where the broadcast power on L1 C/A is increased over certain regions. It is believed that flex power causes the L1 C/A chip shape to be distorted, leading to ranging biases. Because we are evaluating ranging performance for dual frequency ARAIM, the effect on L1 C/A is amplified when making the ionosphere-free combination. This campaign and its effects on the L1 C/A signal has been described in [5]. We seek to observe the effects over long periods. Figure 14 shows the difference between the high rate SU DCB estimates and the CNAV broadcast DCB combination. Some of the error approaches 1 meter on a daily basis due to flex power. As the accuracy of the broadcast orbit and clock increases and the broadcast URA correspondingly decreases, the effects of the DCB error will become relatively more important.
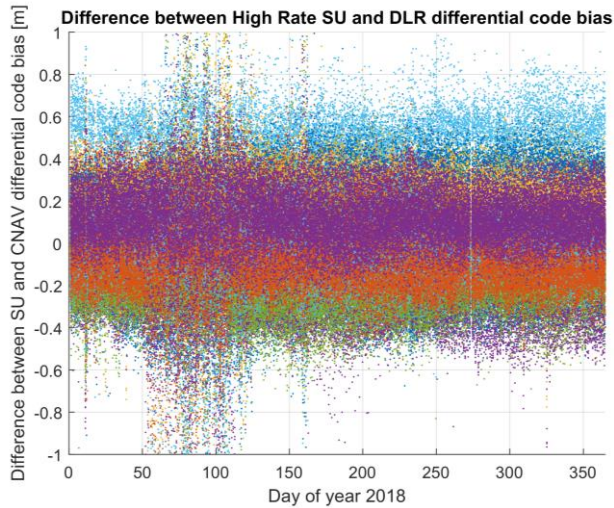
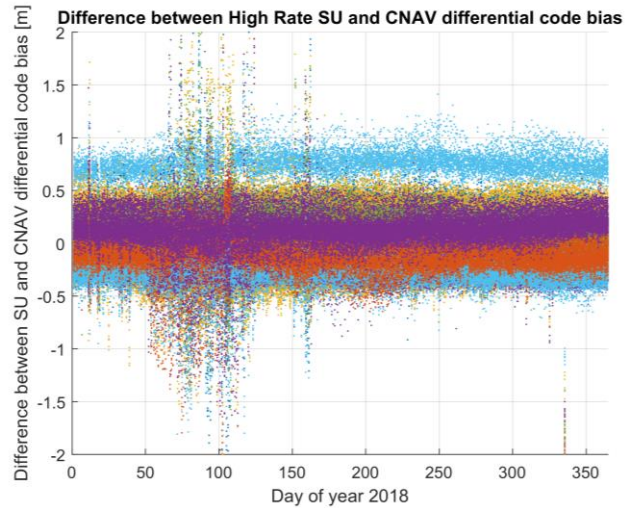*Figure 13: Difference between High Rate SU and DLR DCB*

Figure 14: Difference between High Rate SU and CNAV DCB

Figure 15 shows the significant variation in the DCB due to flex power for PRN 6 across a 5 day period in July 2018. PRN 6 exhibits the most extreme changes, which can be seen in the square wave in the DCB. The broadcast CNAV DCB seems to match when flex power is not used, but when the power is increased, there is a nearly 1 meter ranging difference introduced. This pattern occurs through all of 2018 for many of the IIF satellites.
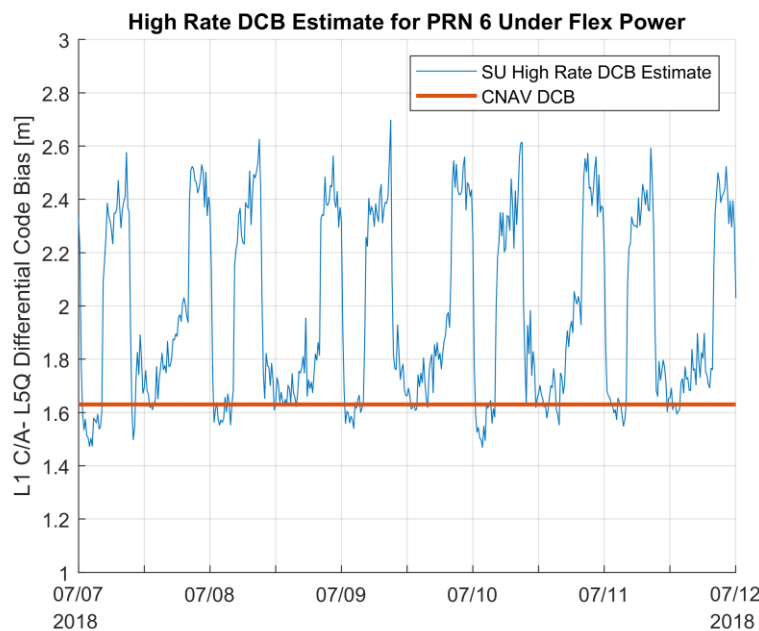

Figure 15: High Rate DCB Estimate for PRN 6 Under Flex Power

The data from Figure 14 is put into histograms for each block IIF satellite and shown in Figure 16. The effect of flex power is immediately clear from the multiple bi-modal distributions present. SVNs 62, 63, 64, 65, 67, 69, 71, and 72 undergo the flex power actions, whereas SVNs 66, 68, 70, and 73 do not. As a result, the four satellites that do not execute flex power have much tighter error distributions when compared to the relatively

much broader distributions of those using flex power. As the capabilities of this tool increase, we will continue to characterize these distributions.
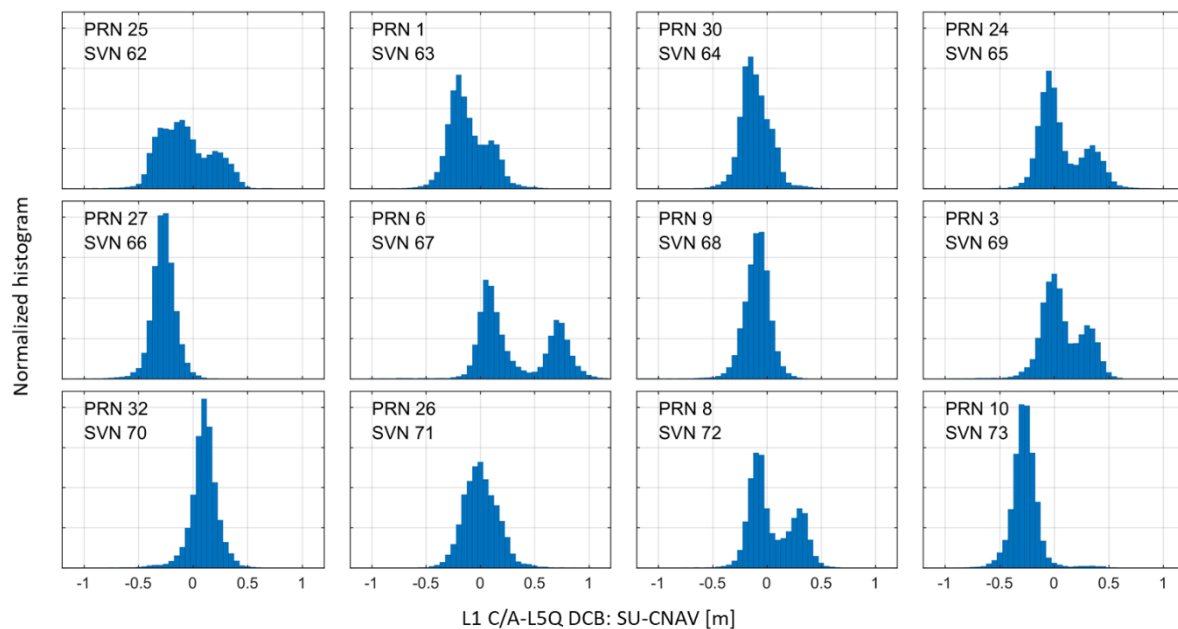

Figure 16: Histogram of Difference between High Rate SU and CNAV DCB

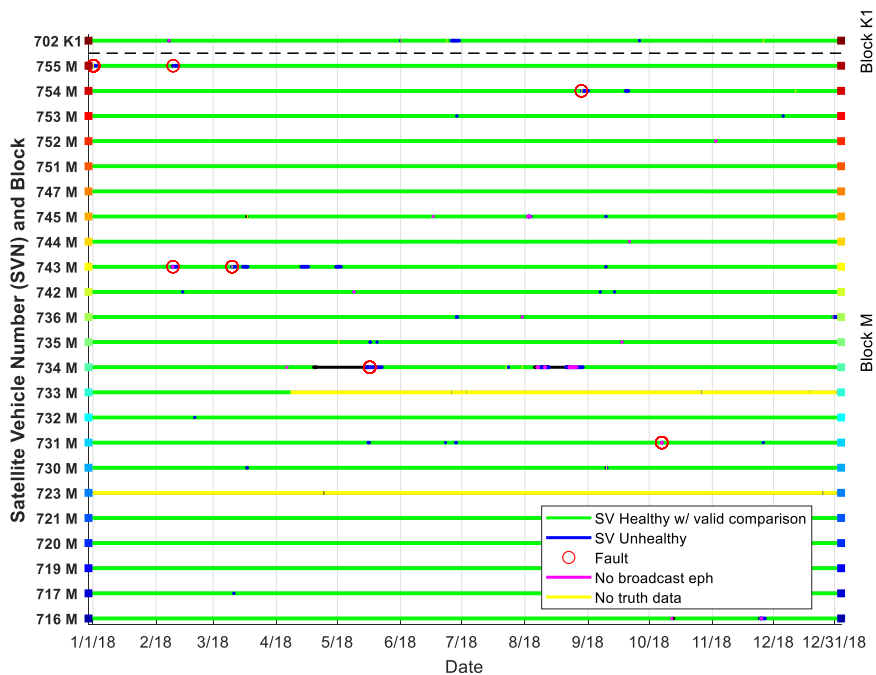**IDENTIFIED GLONASS FAULTS**

Figure 17: GLONASS Performance Overview 2018

The same process that has been used to precisely estimate the clock states of the GPS constellation has also been deployed for GLONASS. Its use for GLONASS is of particular interest because multiple faults occur each year, and often, when they occur, precise clock estimates are unavailable. In this section, we use the SU clock estimation tools to fill in gaps in IGS precise clock availability to better understand the exact nature of GLONASS fault events. Figure 17 shows an overview of GLONASS performance in 2018. This plot has been created through the constellation monitoring process described rigorously in [12], where broadcast navigation logs have been scrubbed in order to be compared to precise ephemeris. Seven fault events have been identified, and three of them will be examined more closely in this section. SVN 723 and SVN 733 both show stretches where "no truth data," or the IGS precise clock and orbit, are available due to a lack of availability of a second broadcast frequency.

Specific fault events in depth:

A fault has been identified on GLONASS SVN 731 on October 7, 2018, as shown in Figure 18. The gray solid, dashed, and dot-dashed lines in the figure indicate the radial, along-track, and cross-track error, respectively. Clock bias error and the maximum projected error (MPE), which is the projected error for a worst-case terrestrial user location, are plotting using the IGS clock bias as well as the SU clock bias. The MPE the value that is actually used for fault identification. The faulted period is indicated by red shading, and the unhealthy period is indicated by the blue shading. The IGS and SU clock bias errors match very closely and are very close to zero throughout the time span. When the satellite is set unhealthy, it does stop broadcasting for a brief period around 6:00. The SU estimates, because they are produced at a higher rate than the 15 minute IGS product, can tell us more accurately the length of the signal outage. In this case, the length does not particularly matter because the satellite was broadcasting an unhealthy flag. One can see that the error consistently crosses zero- this fault is likely caused by incorrect broadcast parameters relating to the propagation of the orbital position. The faulted time, indicated by the red shaded area, lasts 2.5 hours before the satellite is set unhealthy and eventually returned to operation only a short time later.
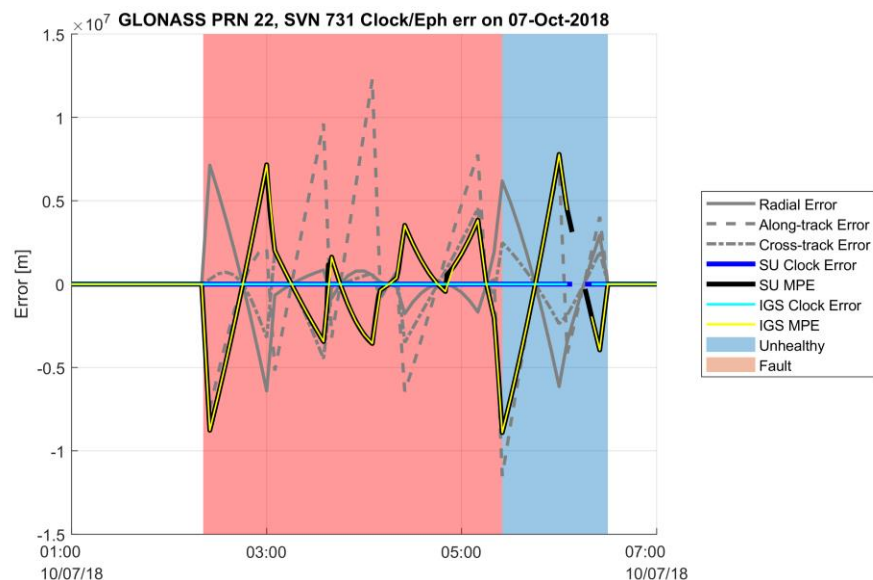

Figure 18: GLONASS Fault Event on PRN 22, 2018-10-07

Figure 19 and Figure 20 show a fault on SVN 754 on August 28, 2018, the cause of which is a frequency jump in the satellite atomic clock. This jump can be seen in particular in Figure 20, which shows the broadcast clock bias as a blue line, and the SU and IGS clock biases as red and teal lines respectively. The IGS product is actually

briefly unavailable at the beginning of the fault. The SU product allows us to better measure the start time of the fault. The precise clock experiences a significant rate jump, whereas the broadcast does not, leading to the fault.
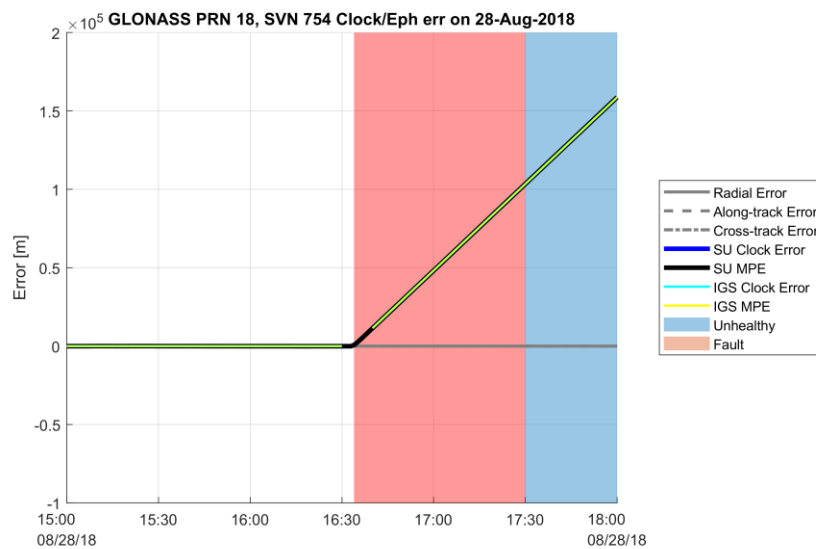

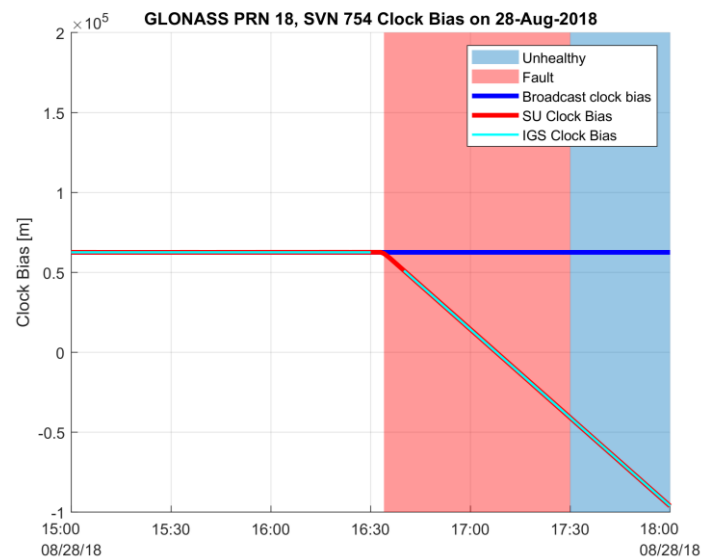*Figure 19: GLONASS Fault Event on PRN 18, 2018-08-28*

Figure 20: Fault event clock bias- precise vs broadcast

The final fault event to be examined occurred on SVN 734 on May 16, 2018. This event occurred as the satellite was set healthy after previously having been set unhealthy. There are significant orbit and clock errors while the satellite is set unhealthy. However, there is a distinct lack of IGS precise clock estimates, which can be seen by the lack of the yellow line indicating the IGS MPE. The SU clock estimate is available through the period without IGS estimates and only stops when the signal becomes unavailable, which is when the fault period ends just after 23:00.
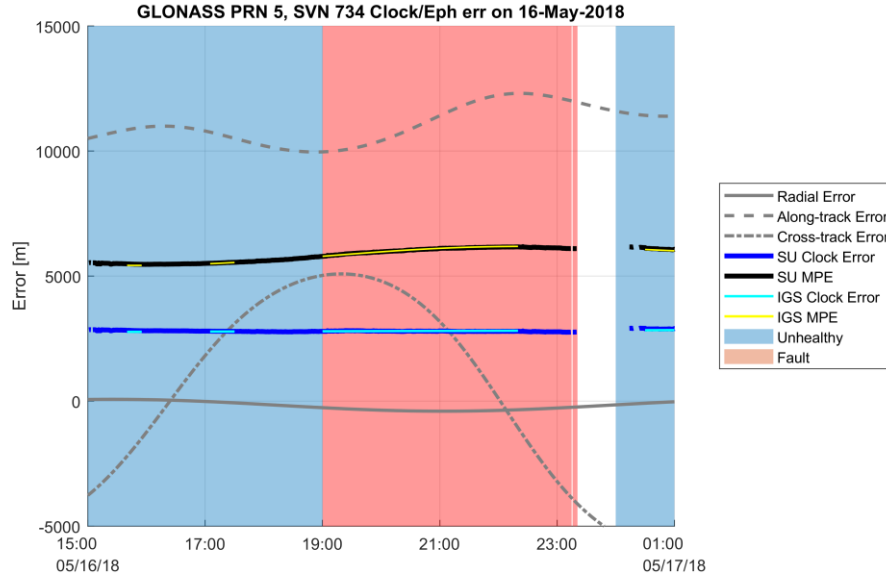
Figure 21: GLONASS Fault Event on PRN 5, 2018-05-16

The full list of identified GLONASS faults is shown in Table 1.

Table 1: List of 2018 GLONASS Faults

PRN	SVN	Start Time	Length (hours)
21	755	01-Jan-2018 01:40:00	7.92
8	743	09-Feb-2018 06:30:00	0.58
21	755	09-Feb-2018 08:50:00	0.33
8	743	10-Mar-2018 06:00:00	1.50
5	734	16-May-2018 19:00:00	4.36
18	754	28-Aug-2018 16:40:00	0.93
22	731	07-Oct-2018 02:30:00	3.06

CONCLUSION

A method for estimating GNSS clock and DCB states has been validated against IGS estimates and found to have sub-decimeter accuracy when comparing using the P1-P2 reference signals. This system has been used to evaluate the ranging performance of the L1 C/A- L5Q dual frequency combination by estimating a separate clock bias and DCB for that signal pair. Daily variations in the clock difference have been observed and linked to the satellite orientation. Daily variations in the DCB have also been observed that have been caused by an ongoing flex power campaign. Finally, the same clock estimation process has been used to closely examine a number of GLONASS faults in 2018.

REFERENCES

[1] Walter, T*., Gunning, K., Eric Phelts, R., and Blanch, J. (2018) Validation of the Unfaulted Error Bounds for ARAIM. J Inst Navig, doi:* 10.1002/navi.214*.*

[2] Gunning, Kazuma, Walter, Todd, Enge, Per, "Characterization of GLONASS Broadcast Clock and Ephemeris: Nominal Performance and Fault Trends for ARAIM," *Proceedings of the 2017 International Technical Meeting of The Institute of Navigation*, Monterey, California, January 2017, pp. 170-183.

[3] Gunning, Kazuma, Walter, Todd, Enge, Per, "Multi-GNSS Constellation Anomaly Detection and Performance Monitoring," *Proceedings of the 30th International Technical Meeting of The Satellite Division of the Institute of Navigation (ION GNSS+ 2017)*, Portland, Oregon, September 2017, pp. 1051-1062.

[4] Wang, Ningbo & Yuan, Yunbin & Li, Zishen & Montenbruck, Oliver & Tan, Bingfeng. (2015). Determination of differential code biases with multi-GNSS observations. Journal of Geodesy. 90. 10.1007/s00190-015-0867-4.

 [5] Steigenberger, Peter & Thölert, Steffen & Montenbruck, Oliver. (2019). Flex power on GPS Block IIR-M and IIF. GPS Solutions. 23. 10.1007/s10291-018-0797-8.

[6] Montenbruck O., Steigenberger P., Prange L., Deng Z., Zhao Q., Perosanz F., Romero I., Noll C., Stürze A., Weber G., Schmid R., MacLeod K., Schaer, S., "The Multi-GNSS Experiment (MGEX) of the International GNSS Service (IGS) – Achievements, Prospects and Challenges", Advances in Space Research 59(7):1671-1697 (2017), DOI: 10.1016/j.asr.2017.01.011 .

[7] I. G. Service. *IGS Antenna Phase Center Offsets*. Available:
       ftp://igscb.jpl.nasa.gov/pub/station/general/igs08.atx

[8] O. Montenbruck *et al.*, "GNSS satellite geometry and attitude models," *Advances in Space Research,* vol. 56, no. 6, pp. 1015-1029, 9/15/ 2015.

[9] A. Hauschild, "Precise GNSS clock-estimation for real-time navigation and Precise Point Positioning," 2011.

[10] IS-GPS-705E

[11] Wang, Ningbo & Yuan, Yunbin & Li, Zishen & Montenbruck, Oliver. (2016). Multi-GNSS differential code biases (DCBs) estimation within MGEX. 10.13140/RG.2.1.3755.6885.

[12] L. Heng, "Safe Satellite Navigation with Multiple Constellations: Global Monitoring of GPS and GLONASS Signal-in-Space Anomalies," 2012.

[13] Montenbruck, Oliver, et al. "Apparent clock variations of the Block IIF-1 (SVN62) GPS satellite." *GPS solutions* 16.3 (2012): 303-313.